Manipulating Core Excitations in Molecules by X-Ray Cavities

Bing Gu[®], ^{1,*} Artur Nenov, ^{2,*} Francesco Segatta, ² Marco Garavelli, ^{2,†} and Shaul Mukamel[®], ¹Department of Chemistry and Department of Physics and Astronomy, University of California, Irvine, California 92697, USA

²Dipartimento di Chimica Industriale "Toso Montanari," Università degli studi di Bologna, Viale del Risorgimento 4, 40136 Bologna, Italy

(Received 27 August 2020; revised 2 December 2020; accepted 22 December 2020; published 4 February 2021)

Core excitations on different atoms are highly localized and therefore decoupled. By placing molecules in an x-ray cavity the core transitions become coupled via the exchange of cavity photons and form delocalized hybrid light-matter excitations known as core polaritons. We demonstrate these effects for the two inequivalent carbon atoms in 1,1-difluoroethylene. Polariton signatures in the x-ray absorption, two-photon absorption, and multidimensional four-wave mixing signals are predicted.

DOI: 10.1103/PhysRevLett.126.053201

Hybrid light-matter states between the material polarization and cavity photon modes, known as polaritons, are created when the light-matter coupling strength is larger than the decay rate of the cavity mode and the decoherence rate of the molecular transition (the strong coupling regime). When the cavity mode is in the vacuum state, the effective coupling strength for an assembly of Nidentical molecules is $\kappa = g\sqrt{N}\mu$, $g \equiv \sqrt{\hbar\omega_c/2\varepsilon_0V_c}$, where ε_0 is the electric permittivity of vacuum, ω_c the cavity frequency, μ the transition dipole moment, and V_c is the cavity mode volume [1]. The \sqrt{N} factor is responsible for cooperative superradiance [2,3]. Cavity polaritons in the visible and infrared regime have long been studied in atoms and were recently experimentally reported in molecules [4–11]. Molecular electronic and vibrational polaritons have been experimentally shown to alter the electronic, optical, and chemical properties of molecules including photoisomerization, electronic energy transfer, electron transfer, and ground-state reaction rates [9]. These findings triggered intensive theoretical investigations [3,6,12–30].

Thin-film optical cavities in the hard x-ray regime have been recently employed in the study of collective Mössbauer signals of ⁵⁷Fe nuclei (14.4 keV) [31–33] and tantalum L-edge x-ray spectra (9881 eV) [34]. A ~ 41 eV effective light-molecule coupling strength for low-finesse x-ray cavities has been reported [34]. X-ray cavities in the soft x-ray regime can be formed by alternating nanometer layers of materials with different indices of refraction, and are on the horizon. For high-reflectivity mirrors, the cavity photon modes satisfy $(n + \frac{1}{2})\lambda_n = L$, where L is the cavity length and λ_n is the wavelength of the cavity mode. For carbon K edge (~300 eV), it corresponds to $L \sim 10$ nm.

Here we study molecular polariton effects in the x-ray regime whereby a high-finesse x-ray cavity mode couples to molecular core excitations. We demonstrate that localized excitations from inequivalent carbon core orbitals in 1,1-difluoroethylene can be coupled by the exchange of an x-ray cavity photon, leading to hybrid core excitation with x-ray cavity photon modes. Rich exciton-polariton physics has been observed in the optical regime. This includes long-range transport [35,36], enhanced optical nonlinearity, modified chemical reactions, polariton lasers, optical transistors, and phase transitions [9]. Our study suggests that similar phenomena may be expected for core polaritons in the x-ray regime. X-ray cavities enable longrange transport of core excitons or core holes despite their highly localized nature as long as the light-matter coupling strength is stronger than their decay rates [35,36]. We predict signatures of core polaritons in the x-ray absorption spectrum, in two-dimensional (2D) x-ray four-wave mixing signals: photon echo (PE) and double quantum coherence (DQC), and in the two-photon absorption. Time-domain 2D spectroscopic techniques provide a versatile tool for exploring the optical properties of matter [37,38]. Multidimensional x-ray spectroscopy enabled by x-ray lasers [39] can [40–42] capture electron dynamics on the attosecond (as) timescale, and can reveal the correlations among core excitations.

We consider a system of N molecules coupled to a single x-ray cavity mode described by the Hamiltonian $H=H_{\rm M}+H_{\rm CM}+H_{\rm LM}(t)+H_{\rm C},$ where the nth molecular Hamiltonian $H_{\rm M}^{(n)}=\sum_{j\in\{g,e,f\}}\hbar\omega_j|j^{(n)}\rangle\langle j^{(n)}|,$ the cavity Hamiltonian $H_{\rm C}=\hbar\omega_c a^\dagger a,$ and the cavity-molecule coupling $H_{\rm CM}=\sum_{n=1}^N-\pmb{\mu}^{(n)}\cdot\hat{\bf E}({\bf r}_n,t).$ Here $\pmb{\mu}^{(n)}$ is the transition dipole moment and $\hat{\bf E}({\bf r})=i\sqrt{\hbar\omega_c/2\varepsilon_0V_c}{\bf e}_cae^{i{\bf k}_c\cdot{\bf r}}+$ H.c. is the electric field operator where $a(a^\dagger)$ is the boson annihilation (creation) operator for the cavity mode, ${\bf k}_c, {\bf e}_c$ are the cavity mode wave vector and polarization, respectively, H.c. stands for the Hermitian conjugate. We focus on the single- and double-core carbon K-edge excited states, labeled e and f, respectively. Double-core excitations of the same carbon atom are excluded, as they are blueshifted by

tens of eV with respect to doubly core-excited states on different atoms [43]. This shift can be attributed to the reduced electron shielding caused by the first core excitation which shifts a second core excitation from the same atom to the blue. The electric-dipole coupling $H_{\rm LM}(t)$ describes the interaction of the molecules with external laser pulses.

For N>1 and $|\mathbf{k}_c\cdot(\mathbf{r}_n-\mathbf{r}_m)|\ll 1$, it is convenient to introduce the collective core-exciton states $|E_{\alpha k}\rangle=(1/\sqrt{N})\sum_{n=1}^N e^{ikn}|g^{(1)}\cdots g^{(n-1)}e_{\alpha}^{(n)}g^{(n+1)}\cdots\rangle$ describing a superposition of a single excitation shared by all molecules and similarly $|F_{\mu k}\rangle$, where $k=2\pi j/N$, $j=0,\ldots,N-1$. Here α and μ run over the singly and doubly excited states, respectively. Up to double excitations, the cavity-molecule coupling can be represented by (see Sec. S1 in Supplemental Material for details [44])

$$H_{\text{CM}} = \sum_{\alpha} \sqrt{N} \kappa_{e_{\alpha}g} |E_{\alpha 0}\rangle \langle G|a + \sum_{k} \sum_{\mu,\alpha} \kappa_{f_{\mu}e_{\alpha}} |F_{\mu k}\rangle \langle E_{\alpha k}|a + \sum_{n \neq m} \sum_{\alpha\beta} \kappa_{e_{\alpha}g} |e_{\alpha}^{(n)} e_{\beta}^{(m)}\rangle \langle e_{\beta}^{(m)}|a + \text{H.c.},$$
(1)

where $|G\rangle=|g^{(1)}\cdots g^{(N)}\rangle$. Equation (1) implies that the transition from the ground state to the delocalized core-exciton states $|E_{a0}\rangle$ is enhanced by \sqrt{N} , whereas the coupling between excited states $|E_{ak}\rangle$ and $|F_{\mu k}\rangle$ does not show such cooperativity [3]. The bright state $|E_{a0}\rangle$ is invariant under exchange of any two molecules. The dark states $|E_{ak}\rangle$, $k\neq 0$ do not contribute to the absorption spectrum. Nevertheless, the transitions between the single-polariton and the dark biexciton states are coupled to the cavity mode by the $|F_{\mu k}\rangle\langle E_{ak}|a+{\rm H.c.}$ term even for $k\neq 0$. Note that bright polariton states can relax to the dark states due to, e.g., vibronic couplings, disorder, and cavity loss [3,59]. The third term in Eq. (1) represents the coupling between the singly and doubly core-excited states from different molecules (Sec. S1 of Supplemental Material [44]).

Figure 1 depicts the ground-state structure of 1,1difluoroethylene optimized at the Møller-Plesset secondorder perturbation level, and compares the simulated and experimental x-ray absorption near edge structure (XANES) in the [280, 296] eV spectral range. This molecule has two inequivalent carbon atoms with bound preedge transitions separated by a few eV. The electronic structure computations are detailed in Sec. S2 and the spectroscopic simulations in Sec. S3 [44] The simulated XANES spectrum (without any shift) is in excellent agreement with experiment in the [280, 296] eV spectral range. The spectrum has four main features. The 285.6 and 289.5 eV peaks are associated with excitations from the 1s core orbitals of the carbon atoms in the CH₂ and CF₂ groups to the antibonding π^* orbital, respectively. A broader peak at 293 eV arises from a pair of close lying

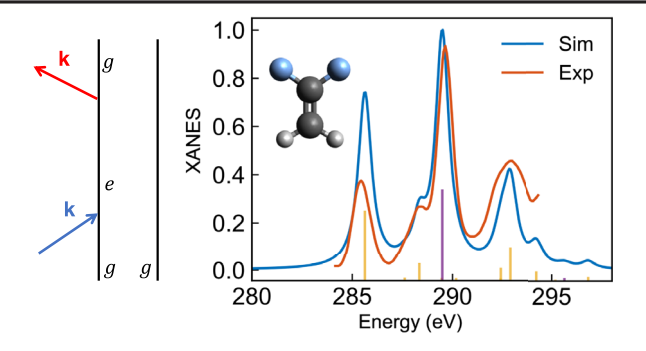


FIG. 1. The XANES spectrum of 1,1-difluoroethylene and the corresponding (left) Feynman diagram. \mathbf{k} denotes the incoming pulse wave vector. Right: The transitions involving the carbon K-edge in CH_2 (CF_2) are represented by yellow (purple) sticks. The agreement with experiment [60] is excellent.

transitions from CH₂ to Rydberg (Ry) orbitals. Finally, we find a red shoulder to the 289.5 eV band at 288.4 eV, associated with a transition from CH₂ to a σ^* antibonding orbital localized in the CH₂ fragment. The ~4 eV energy splitting between the CH₂ $\rightarrow \pi^*$ and CF₂ $\rightarrow \pi^*$ peaks shows that functionalization with electron withdrawing groups such as fluorine makes core excitations more energy costly, thus inducing a few eV blueshift. The *K*-edge spectrum is dominated by the core excitations of CH₂.

In the x-ray cavity, the core excitations are modified by coupling to the cavity mode. Figure 2 (top) illustrates the XANES of core polaritons at cavity frequencies $\omega_c=290$ eV close to the $\mathrm{CF}_2 \to \pi^*$ excitation for varying coupling strength. At $g\sqrt{N}=2.45$ eV/D, we observe a vacuum Rabi splitting of two polariton peaks. The transition dipole is in the order of 0.1 D. The Rabi splitting is increased with the coupling strength, and the lower polariton further mixes with CH_2 excitations leading to enhancement and redshift of the $\mathrm{CH}_2 \to \pi^*$ transition.

To unveil the polaritonic nature of the core excitations in the x-ray cavity, we have decomposed each polariton state into the CH₂, CF₂, and the cavity photon components. These are depicted in the lower panels in Fig. 2. Since the core excitations localized at CH₂ and CF₂ are decoupled, each excitation is either purely CH2 or CF₂ type. To decompose the polariton states, we introduce the projection operators $P_{\sigma} = \sum_{\alpha \in \sigma} |e_{\alpha}\rangle\langle e_{\alpha}|,$ where $\sigma = \{\text{cavity photon}, \text{CH}_2, \text{CF}_2\}$. The σ component in a polariton state $|\Psi\rangle$ is computed as $\langle \Psi|P_{\sigma}|\Psi\rangle$. As shown in Fig. 2, without cavity (g = 0), all excitations are either purely CH₂ (yellow) or CF₂ (purple) type. As the coupling is turned on, the two ~290 eV excitations contain mixed CF₂ and photon (brown) character, reflecting a hybridization of the $CF_2 \rightarrow \pi^*$ and the cavity photon, resembling the polariton states in a Jaynes-Cummings model. As q increases, the polariton states further mix with CH₂ excitations, leading to delocalized core excitations from both CH₂ and CF₂. The delocalization can be

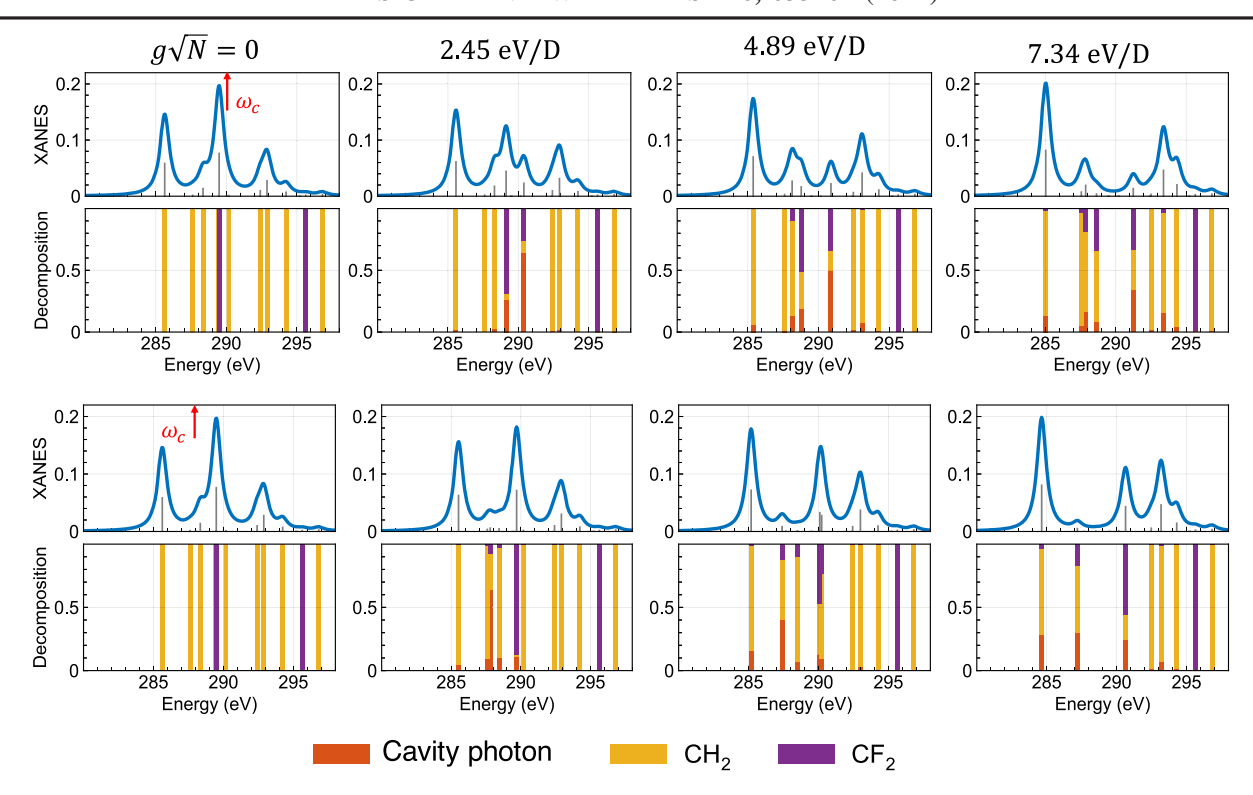


FIG. 2. XANES of 1,1-difluoroethylene in an x-ray cavity for varying coupling strength. Lower panels show the decomposition of each polariton state into CH₂, CF₂, and photon components. The top row is for cavity frequency $\omega_c = 290$ eV close to a specific transition, and the bottom row for cavity frequency $\omega_c = 288$ eV detuned from the main core transitions. The dependence on N is solely through the (collective) coupling strength $q\sqrt{N}$.

clearly observed in the decomposition of the polariton states ~290 eV. These delocalized excitations involving both C atoms arise from an effective coupling between their core excitations induced by exchanging cavity photons even when the cavity is in the vacuum state. When the cavity frequency is detuned far from any resonance in the bare XANES $\omega_c = 288$ eV (bottom row of Fig. 2), no substantial changes in the spectrum are observed at g = 2.45 eV/D. Nevertheless, as g gets stronger, we observe similar delocalized core excitations involving both CH₂ and CF₂ at, e.g., 290 eV.

For nonlinear x-ray signals, we focus on the single-molecule N=1 strong coupling case. Single-molecule strong coupling requires a substantial field enhancement, and its realization may benefit from an ensemble of auxiliary emitters [61]. The signals for large N can depend on many collective dark states that are neglected here. Doubly core-excited dark states $|e_{\alpha}^{(n)}e_{\beta}^{(m)}\rangle$ in different molecules also need to be taken into account. Such states do not show up in bare nonlinear spectroscopy due to destructive interference [62,63]. The cavity mode mediates an effective coupling even for otherwise noninteracting molecules, and the two-core-exciton states from different molecules will influence the bipolariton manifold. Below, g, e, f label the ground, single-polariton, and two-polariton states, respectively; see Fig. 3 for the level scheme.

We have computed time-domain heterodyne-detected 2D x-ray four-wave mixing signals of core polaritons. These allow us to track the time evolution of the polariton states and reveal correlations between transitions. The total electric field is decomposed into three pulses, $E(t) = E_3(t) + E_2(t+T_2) + E_1(t+T_1+T_2) + \text{c.c.}$, where T_j is the time delay between the jth and (j+1)th pulse. Labeling the wave vectors of the incoming pulses as \mathbf{k}_j , we first discuss photon echo signal at $-\mathbf{k}_1 + \mathbf{k}_2 + \mathbf{k}_3$.

The 2D PE spectra are sketched by the Liouville space pathways represented by Feynman diagrams [37], depicted in Fig. S1 of Supplemental Material [44]. The 2D correlation spectra are obtained by Fourier transforming the delays T_1 (coherence time) and $T_3 \equiv t$ (detection time) in the polarization $S_{\rm PE}(\Omega_3, \Omega_1; T_2) = \int_0^\infty dT_1 \int_0^\infty dT_3 \langle P_{\rm PE}(T_3, T_2, T_1) \rangle e^{i\Omega_3 T_3 + i\Omega_1 T_1}$.

The 2D PE signals are displayed in Fig. 3. There are three contributions to the spectra: stimulated emission (SE) and ground-state bleaching (GSB) (the first two diagrams in Fig. S1 [44]) and the excited state absorption (ESA) (the last diagram in Fig. S1 [44]). The four XANES features discussed earlier give rise to four traces along Ω_1 (i.e., CH₂ excitations at 285.6, 288.4, and 293.0 eV and CF₂ excitations at 289.5 eV) with a characteristic cross peak pattern, that reflects the correlation between various transitions. The cross peaks result from the fact that they share a common

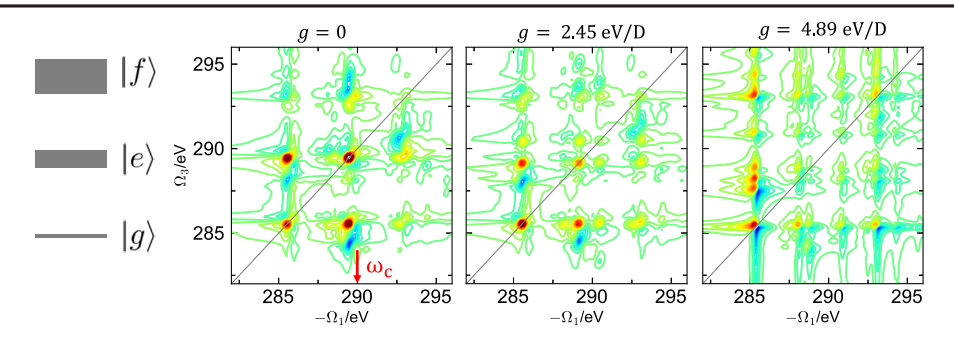


FIG. 3. Level scheme and the 2D photon echo spectra $S_{PE}(\Omega_3, \Omega_1; T_2 = 0)$ for 1,1-difluoroethylene in an x-ray cavity with $\omega_c = 290$ eV for different coupling strengths as indicated. We use attosecond pulses with central frequency 290 and 20 eV bandwidth.

ground state, and that the core excitations are both anharmonic $\omega_{fe} \neq \omega_{eq}$ and coupled $\omega_{fq} \neq \omega_{eq} + \omega_{e'q}$. ESA signals related to double core excitations from the same carbon atom do not cancel the respective GSB and SE signals, consequently, cross peaks appear symmetrically below and above the diagonal. Transitions involving CH₂ and CF₂ cores are quartically coupled due to spatial vicinity of the two carbons; i.e., excitations of CH₂ core depends on the occupation number in CF₂ and vice versa. The associated ESA exhibit a ~1.5 eV redshift $(\Omega_1, \Omega_3) =$ (289.6 eV, 284.0 eV) and (285.6 eV, 288.0 eV) or a blueshift (289.6 eV, 294.5 eV) and (293.0 eV, 291.0 eV) with respect to the corresponding off-diagonal GSB which makes the ESA appear in the 2D spectra. At q = 2.45 eV/D, the polariton splitting is reflected in the additional cross peaks between the polariton states and bare molecular states. Similar features are seen in the stronger coupling case shown in Fig. 3 where additional hybrid polariton states containing excitations from both carbon atoms are created.

We now turn to the DQC signal at $\mathbf{k}_1 + \mathbf{k}_2 - \mathbf{k}_3$ [64–68], represented by the diagrams shown in Fig. S2 [44]. The correlations between single and two polaritons can be obtained either by Fourier transform of the time delays T_3 and T_2 at a fixed T_1 , $S_{DOC}(\Omega_3, \Omega_2; T_1)$ or by Fourier transform of the time delays T_1 and T_2 at a fixed T_3 $S_{\rm DOC}(\Omega_2,\Omega_1;T_3)$. In DQC, the polariton system is in the coherence $|e\rangle\langle g|$ during T_1 , and is then promoted to $|f\rangle\langle g|$ during T_2 . The system can be either $|f\rangle\langle e|$ or $|e\rangle\langle g|$ for the detection time T_3 . The peaks in $S_{DQC}(\Omega_2, \Omega_1; T_3)$ reveal correlation between ω_{eq} and ω_{fq} . For a harmonic system where $\omega_{fg}=\omega_{eg}$ and for uncorrelated transitions where $\omega_{fg} = \omega_{eg} + \omega_{e'g}$, the DQC signal vanishes as the two contributions to DQC interfere destructively. This makes DQC suitable for resolving anharmonicities and correlated transitions.

The DQC $S_{\mathrm{DQC}}(\Omega_2,\Omega_1;T_3)$ are shown in Fig. 4 for varying cavity coupling strengths. The vertical axis shows the doubly core-excited states $|f\rangle$ that can be reached from $|g\rangle$ through an excited state $|e\rangle$. Prominent contributions at $(\Omega_1,\Omega_2)=(285.6 \ \mathrm{eV},573.9 \ \mathrm{eV})$ and

(289.5 eV, 573.9 eV) arise due to the coupling of $\text{CH}_2 \rightarrow \pi^* \ (285.6 \ \text{eV}) \ \text{and} \ \text{CF}_2 \rightarrow \pi^* \ (289.5 \ \text{eV}) \ \text{transport}$ sitions to the CH₂, CF₂ $\Rightarrow \pi^*$ transition [69]. Similarly, peaks at (289.5 eV, 584.1 eV) and (293.0 eV, 584.1 eV) arise due to the coupling of $CF_2 \rightarrow \pi^*$ (289.5 eV) and $CH_2 \rightarrow Ry (293.0 \text{ eV})$ transitions to the CH_2 , $CF_2 \Rightarrow \pi^*$, Ry transition. In the strong coupling regime, the polariton states manifest as a doublet around $\Omega_1 = 290$ eV. Additional peaks are clearly observed between these single-polariton states and the f manifold. Core polaritons also modulate the doubly core-excited states by mixing them with the two-cavity-photon state and singlecore-excitation single-cavity-photon state. For example, a noticeable redshift can be observed for the CH₂, $CF_2 \Rightarrow \pi^*$ transition from the slices of the DQC at $\Omega_1 = 285.5 \text{ eV}$.

The correlations between ω_{fe} and ω_{fg} are revealed in the DQC signal $S_{\text{DOC}}(\Omega_3, \Omega_2; T_1)$ displayed in Fig. 4 (bottom

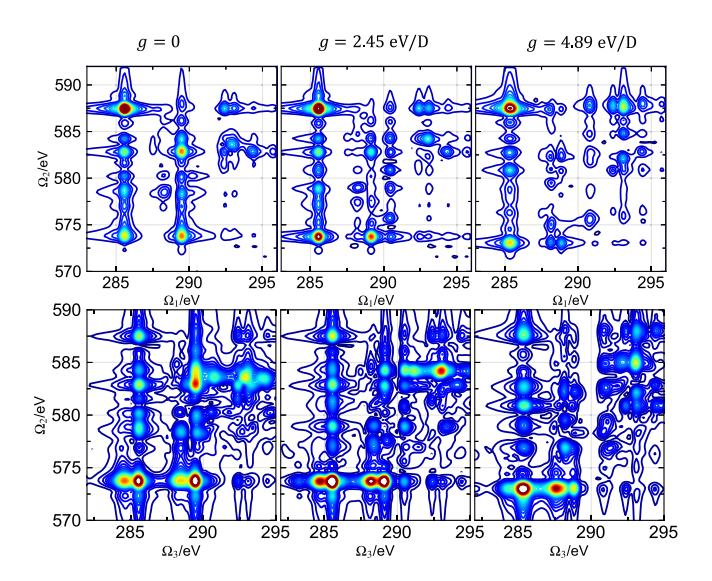


FIG. 4. 2D double quantum coherence spectra $|S_{\mathrm{DQC}}(\Omega_2,\Omega_1;T_3)|$ (upper row) and $|S_{\mathrm{DQC}}(\Omega_3,\Omega_2;T_1)|$ (lower row) in an x-ray cavity with $\omega_c=290$ eV at different coupling strengths g as indicated. A small time delay 10^{-5} as is used for both T_3 and T_1 to avoid cancellation of the two DQC diagrams.

row). States from the doubly excited manifold coupled to the singly excited manifold are characterized through a set of four peaks along Ω_3 for a given Ω_2 value [70]. For example, the quartet of peaks along the $\Omega_2=573.9$ eV are associated with two peaks at 285.6 eV and 289.5 eV coinciding with the $CH_2 \rightarrow \pi^*$ and $CF_2 \rightarrow \pi^*$ transitions and two red-shifted peaks at 284.4 and 288.3 eV corresponding to the $CH_2 \rightarrow \pi^*$ with CF_2 excited and $CF_2 \rightarrow \pi^*$ with CH_2 excited [71]. The 1.2 eV splitting corresponds to the value of the quartic coupling between both transitions. Under strong coupling, core-polariton doublets can be observed along Ω_3 due to the ω_{fe} resonances. The splitting does not directly correspond to the polariton resonances because both e and f manifolds are modified by the cavity mode.

Similar information about the correlations of single and double excitations as provided by DQC can be extracted from the two-photon absorption signal, discussed in Sec. S4 of Supplemental Material [44]. This signal does not require coherent x-ray pulses and is thus easier to implement experimentally.

In summary, we have demonstrated how molecular core excitations can be manipulated by coupling to the vacuum field in an x-ray cavity. Localized excitations from the two carbon atoms in 1,1-difluoroethylene are coherently coupled by the exchange of an x-ray cavity photon creating hybrid delocalized excitations. We identified the spectroscopic signatures of core polaritons in XANES, two-photon absorption, and multidimensional x-ray spectroscopic signals. XANES directly probes the hybrid core-polariton states with the polariton effects manifested as mode splitting, redistribution of oscillator strength, and line shifts, depending on the cavity frequency and coupling strength. Correlations between polaritonic excitations are revealed by the PE, and information about the two-polariton manifold can be readily extracted from the DQC and two-photon absorption signals. This study shows how to manipulate core excitations in molecules by strong coupling to a cavity in the x-ray regime. Many interesting phenomena discovered for exciton polaritons in the optical regime such as long-range transport [35], modified chemical reaction rates [72], and enhanced nonlinearity [36] suggest analogous extensions for core polaritons in the xray regime. Relaxation dynamics of core polaritons is also expected to differ significantly from the bare core excitations. Collective effects found in Mössbauer resonance in iron including electromagnetically induced transparency and Lamb shift [32,33] may show up in molecules as well.

We thank Dr. Stefano M. Cavaletto for helpful discussions and Dr. Ralf Röhlsberger for valuable feedback. M. G., A. N., F. S., and S. M. acknowledge support from the Chemical Sciences, Geosciences, and Bio-sciences division, Office of Basic Energy Sciences, Office of Science, U.S. Department of Energy, through Award

No. DE-SC0019484. B. G. acknowledges the support from the National Science Foundation Grant No. CHE-1953045.

- These authors contributed equally to this work.
- marco.garavelli@unibo.it
- *smukamel@uci.edu
- [1] E. M. Purcell, Spontaneous emission probabilities at radio frequencies, Phys. Rev. 69, 681 (1946), http://pages.erau .edu/~reynodb2/colloquia/ Purcell_1946_SpontaneousEmission.pdf.
- [2] R. H. Dicke, Coherence in spontaneous radiation processes, Phys. Rev. 93, 99 (1954).
- [3] M. Kowalewski, K. Bennett, and S. Mukamel, Femtochemistry: Manipulating nonadiabatic dynamics at avoided crossings, J. Phys. Chem. Lett. 7, 2050 (2016).
- [4] X. Zhong, T. Chervy, L. Zhang, A. Thomas, J. George, C. Genet, J. A. Hutchison, and T. W. Ebbesen, Energy transfer between spatially separated entangled molecules, Angew. Chem., Int. Ed. Engl. 56, 9034 (2017).
- [5] J. George, A. Shalabney, J. A. Hutchison, C. Genet, and T. W. Ebbesen, Liquid-phase vibrational strong coupling, J. Phys. Chem. Lett. 6, 1027 (2015).
- [6] A. Shalabney, J. George, J. Hutchison, G. Pupillo, C. Genet, and T. W. Ebbesen, Coherent coupling of molecular resonators with a microcavity mode, Nat. Commun. 6, 5981 (2015).
- [7] F. Benz, M. K. Schmidt, A. Dreismann, R. Chikkaraddy, Y. Zhang, A. Demetriadou, C. Carnegie, H. Ohadi, B. de Nijs, R. Esteban, J. Aizpurua, and J. J. Baumberg, Singlemolecule optomechanics in "picocavities", Science 354, 726 (2016).
- [8] K. Y. Yang, D. Y. Oh, S. H. Lee, Q.-F. Yang, X. Yi, B. Shen, H. Wang, and K. Vahala, Bridging ultrahigh-Q devices and photonic circuits, Nat. Photonics 12, 297 (2018).
- [9] T. W. Ebbesen, Hybrid light–matter states in a molecular and material science perspective, Acc. Chem. Res. 49, 2403 (2016).
- [10] X. Zhong, T. Chervy, S. Wang, J. George, A. Thomas, J. A. Hutchison, E. Devaux, C. Genet, and T. W. Ebbesen, Nonradiative energy transfer mediated by hybrid light-matter states, Angew. Chem. 128, 6310 (2016).
- [11] R. Chikkaraddy, B. de Nijs, F. Benz, S. J. Barrow, O. A. Scherman, E. Rosta, A. Demetriadou, P. Fox, O. Hess, and J. J. Baumberg, Single-molecule strong coupling at room temperature in plasmonic nanocavities, Nature (London) 535, 127 (2016).
- [12] B. Gu and S. Mukamel, Manipulating nonadiabatic conical intersection dynamics by optical cavities, Chem. Sci. 11, 1290 (2020).
- [13] M. Kowalewski, K. Bennett, J. R. Rouxel, and S. Mukamel, Monitoring Nonadiabatic Electron-Nuclear Dynamics in Molecules by Attosecond Streaking of Photoelectrons, Phys. Rev. Lett. 117, 043201 (2016).
- [14] K. Bennett, M. Kowalewski, and S. Mukamel, Novel photochemistry of molecular polaritons in optical cavities, Faraday Discuss. 194, 259 (2016).
- [15] C. Schäfer, M. Ruggenthaler, H. Appel, and A. Rubio, Modification of excitation and charge transfer in cavity

- quantum-electrodynamical chemistry, Proc. Natl. Acad. Sci. U.S.A. **116**, 4883 (2019).
- [16] J. Galego, F. J. Garcia-Vidal, and J. Feist, Cavity-Induced Modifications of Molecular Structure in the Strong-Coupling Regime, Phys. Rev. X 5, 041022 (2015).
- [17] J. Flick, M. Ruggenthaler, H. Appel, and A. Rubio, Atoms and molecules in cavities, from weak to strong coupling in quantum-electrodynamics (QED) chemistry, Proc. Natl. Acad. Sci. U.S.A. 114, 3026 (2017).
- [18] J. Flick, N. Rivera, and P. Narang, Strong light-matter coupling in quantum chemistry and quantum photonics, Nanophotonics 7, 1479 (2018).
- [19] K. E. Dorfman and S. Mukamel, Multidimensional photon correlation spectroscopy of cavity polaritons, Proc. Natl. Acad. Sci. U.S.A. 115, 1451 (2018).
- [20] F. Herrera and F. C. Spano, Absorption and photoluminescence in organic cavity QED, Phys. Rev. A 95, 053867 (2017).
- [21] D. M. Coles, N. Somaschi, P. Michetti, C. Clark, P. G. Lagoudakis, P. G. Savvidis, and D. G. Lidzey, Polaritonmediated energy transfer between organic dyes in a strongly coupled optical microcavity, Nat. Mater. 13, 712 (2014).
- [22] A. F. Kockum, A. Miranowicz, S. De Liberato, S. Savasta, and F. Nori, Ultrastrong coupling between light and matter, Nat. Rev. Phys. 1, 19 (2019).
- [23] P. Vasa and C. Lienau, Strong light-matter interaction in quantum emitter/metal hybrid nanostructures, ACS Photonics 5, 2 (2018).
- [24] M. Hertzog, M. Wang, J. Mony, and K. Börjesson, Strong light–matter interactions: A new direction within chemistry, Chem. Soc. Rev. 48, 937 (2019).
- [25] T. Schwartz, J. A. Hutchison, J. Léonard, C. Genet, S. Haacke, and T. W. Ebbesen, Polariton dynamics under strong light-molecule coupling, Chem. Phys. Chem. 14, 125 (2013).
- [26] F. Herrera and F. C. Spano, Dark Vibronic Polaritons and the Spectroscopy of Organic Microcavities, Phys. Rev. Lett. 118, 223601 (2017).
- [27] L. A. Martínez-Martínez, M. Du, R. F. Ribeiro, S. Kéna-Cohen, and J. Yuen-Zhou, Polariton-assisted singlet fission in acene aggregates, J. Phys. Chem. Lett. 9, 1951 (2018).
- [28] D. Sanvitto and S. Kéna-Cohen, The road towards polaritonic devices, Nat. Mater. **15**, 1061 (2016).
- [29] B. Gu and S. Mukamel, Manipulating two-photonabsorption of cavity polaritons by entangled light, J. Phys. Chem. Lett. **11**, 8177 (2020).
- [30] A. Mandal and P. Huo, Investigating new reactivities enabled by polariton photochemistry, J. Phys. Chem. Lett. 10, 5519 (2019).
- [31] R. Röhlsberger, J. Evers, and S. Shwartz, Quantum and nonlinear optics with hard x-rays, in *Synchrotron Light Sources and Free-Electron Lasers*, edited by E. J. Jaeschke, S. Khan, J. R. Schneider, and Jerome B. Hastings (Springer International Publishing, Cham, 2020), pp. 1399–1431.
- [32] R. Rohlsberger, K. Schlage, B. Sahoo, S. Couet, and R. Ruffer, Collective lamb shift in single-photon superradiance, Science **328**, 1248 (2010).
- [33] R. Röhlsberger, H.-C. Wille, K. Schlage, and B. Sahoo, Electromagnetically induced transparency with resonant nuclei in a cavity, Nature (London) 482, 199 (2012).

- [34] J. Haber, J. Gollwitzer, S. Francoual, M. Tolkiehn, J. Strempfer, and R. Röhlsberger, Spectral Control of an X-Ray *L*-Edge Transition via a Thin-Film Cavity, Phys. Rev. Lett. **122**, 123608 (2019).
- [35] G. G. Rozenman, K. Akulov, A. Golombek, and T. Schwartz, Long-range transport of organic exciton-polaritons revealed by ultrafast microscopy, ACS Photonics **5**, 105 (2018).
- [36] T. Chervy, J. Xu, Y. Duan, C. Wang, L. Mager, M. Frerejean, J. A. W. Münninghoff, P. Tinnemans, J. A. Hutchison, C. Genet, A. E. Rowan, T. Rasing, and T. W. Ebbesen, Highefficiency second-harmonic generation from hybrid lightmatter states, Nano Lett. 16, 7352 (2016).
- [37] S. Mukamel, *Principles of Nonlinear Optical Spectroscopy* (Oxford University Press, Oxford, 1995).
- [38] B. Xiang, R. F. Ribeiro, A. D. Dunkelberger, J. Wang, Y. Li, B. S. Simpkins, J. C. Owrutsky, J. Yuen-Zhou, and W. Xiong, Two-dimensional infrared spectroscopy of vibrational polaritons, Proc. Natl. Acad. Sci. U.S.A. 115, 4845 (2018)
- [39] C. Pellegrini, A. Marinelli, and S. Reiche, The physics of x-ray free-electron lasers, Rev. Mod. Phys. **88**, 015006 (2016).
- [40] S. Mukamel, D. Healion, Y. Zhang, and J. D. Biggs, Multidimensional attosecond resonant x-ray spectroscopy of molecules: Lessons from the optical regime, Annu. Rev. Phys. Chem. **64**, 101 (2013).
- [41] S. Tanaka and S. Mukamel, X-ray four-wave mixing in molecules, J. Chem. Phys. 116, 1877 (2002).
- [42] J. D. Biggs, Y. Zhang, D. Healion, and S. Mukamel, Two-dimensional stimulated resonance Raman spectroscopy of molecules with broadband x-ray pulses, J. Chem. Phys. **136**, 174117 (2012).
- [43] A. Nenov, F. Segatta, A. Bruner, S. Mukamel, and M. Garavelli, X-ray linear and non-linear spectroscopy of the ESCA molecule, J. Chem. Phys. 151, 114110 (2019).
- [44] See Supplemental Material at http://link.aps.org/supplemental/10.1103/PhysRevLett.126.053201 for details of the electronic structure and spectroscopic computations, which includes Refs. [45–58].
- [45] N. Forsberg and P.-A. Malmqvist, Multiconfiguration perturbation theory with imaginary level shift, Chem. Phys. Lett. 274, 196 (1997).
- [46] P.-A. Malmqvist, A. Rendell, and B. O. Roos, The restricted active space self-consistent-field method, implemented with a split graph unitary group approach, J. Phys. Chem. **94**, 5477 (1990).
- [47] M. Lundberg and M. G. Delcey, Multiconfigurational Approach to x-ray spectroscopy of transition metal complexes, in *Transition Metals in Coordination Environments*, edited by E. Broclawik, T. Borowski, and M. Radoń (Springer International Publishing, New York, 2019).
- [48] K. Andersson, P.-A. Malmqvist, B. O. Roos, A. J. Sadlej, and K. Wolinski, Second-order perturbation theory with a CASSCF reference function, J. Phys. Chem. **94**, 5483 (1990).
- [49] V. Sauri, L. Serrano-Andrés, A. R. M. Shahi, L. Gagliardi, S. Vancoillie, and K. Pierloot, Multiconfigurational secondorder perturbation theory restricted active space (RASPT2)

- method for electronic excited states: A benchmark study, J. Chem. Theory Comput. **7**, 153 (2011).
- [50] D. Roca-Sanjuán, F. Aquilante, and R. Lindh, Multiconfiguration second-order perturbation theory approach to strong electron correlation in chemistry and photochemistry, Comput. Mol. Sci. 2, 585 (2012).
- [51] G. Ghigo, B. O. Roos, and P.-A. Malmqvist, A modified definition of the zeroth-order Hamiltonian in multiconfigurational perturbation theory (CASPT2), Chem. Phys. Lett. 396, 142 (2004).
- [52] J. P. Zobel, J. J. Nogueira, and L. González, The IPEA dilemma in CASPT2, Chem. Sci. 8, 1482 (2017).
- [53] T. B. Pedersen, F. Aquilante, and R. Lindh, Density fitting with auxiliary basis sets from Cholesky decompositions, Theor. Chem. Acc. 124, 1 (2009).
- [54] M. Kowalewski, B. P. Fingerhut, K. E. Dorfman, K. Bennett, and S. Mukamel, Simulating coherent multidimensional spectroscopy of nonadiabatic molecular processes: From the infrared to the x-ray regime, Chem. Rev. 117, 12165 (2017).
- [55] B. O. Roos, V. Veryazov, and P.-O. Widmark, Relativistic atomic natural orbital type basis sets for the alkaline and alkaline-earth atoms applied to the ground-state potentials for the corresponding dimers, Theor. Chem. Acc. 111, 345 (2004).
- [56] I. F. Galván et al., OpenMolcas: From source code to insight, J. Chem. Theory Comput. 15, 5925 (2019).
- [57] F. Aquilante et al., Modern quantum chemistry with [Open] Molcas, J. Chem. Phys. 152, 214117 (2020).
- [58] K. E. Dorfman and S. Mukamel, Nonlinear spectroscopy with time- and frequency-gated photon counting: A superoperator diagrammatic approach, Phys. Rev. A 86, 013810 (2012).
- [59] C. A. DelPo, B. Kudisch, K. H. Park, S.-U.-Z. Khan, F. Fassioli, D. Fausti, B. P. Rand, and G. D. Scholes, Polariton transitions in femtosecond transient absorption studies of ultrastrong light–molecule coupling, J. Phys. Chem. Lett. 11, 2667 (2020).
- [60] R. McLaren, S. A. C. Clark, I. Ishii, and A. P. Hitchcock, Absolute oscillator strengths from *K*-shell electron-energyloss spectra of the fluoroethenes and 1,3-perfluorobutadiene, Phys. Rev. A **36**, 1683 (1987).

- [61] S. Schütz, J. Schachenmayer, D. Hagenmüller, G. K. Brennen, T. Volz, V. Sandoghdar, T. W. Ebbesen, C. Genes, and G. Pupillo, Ensemble-Induced Strong Light-Matter Coupling of a Single Quantum Emitter, Phys. Rev. Lett. 124, 113602 (2020).
- [62] A. Muthukrishnan, G. S. Agarwal, and M. O. Scully, Inducing Disallowed Two-Atom Transitions with Temporally Entangled Photons, Phys. Rev. Lett. 93, 093002 (2004).
- [63] M. Richter and S. Mukamel, Collective two-particle resonances induced by photon entanglement, Phys. Rev. A 83, 063805 (2011).
- [64] M. Richter and S. Mukamel, Ultrafast double-quantumcoherence spectroscopy of excitons with entangled photons, Phys. Rev. A 82, 013820 (2010).
- [65] I. V. Schweigert and S. Mukamel, Double-quantum-coherence attosecond x-ray spectroscopy of spatially separated, spectrally overlapping core-electron transitions, Phys. Rev. A **78**, 052509 (2008).
- [66] J. Kim, S. Mukamel, and G. D. Scholes, Two-dimensional electronic double-quantum coherence spectroscopy, Acc. Chem. Res. **42**, 1375 (2009).
- [67] X. Dai, M. Richter, H. Li, A. D. Bristow, C. Falvo, S. Mukamel, and S. T. Cundiff, Two-Dimensional Double-Quantum Spectra Reveal Collective Resonances in an Atomic Vapor, Phys. Rev. Lett. 108, 193201 (2012).
- [68] D. Abramavicius, A. Nemeth, F. Milota, J. Sperling, S. Mukamel, and H. F. Kauffmann, Weak Exciton Scattering in Molecular Nanotubes Revealed by Double-Quantum Two-Dimensional Electronic Spectroscopy, Phys. Rev. Lett. 108, 067401 (2012).
- [69] Here, \Rightarrow indicates a double excitation.
- [70] A. Nenov, I. Rivalta, S. Mukamel, and M. Garavelli, Bidimensional electronic spectroscopy on indole in gas phase and in water from first principles, Comput. Theor. Chem., 1040–1041, 295 (2014).
- [71] Here, the brackets indicate that the core-excitation occurs in the presence of a core-excited carbon.
- [72] J. A. Hutchison, T. Schwartz, C. Genet, E. Devaux, and T. W. Ebbesen, Modifying chemical landscapes by coupling to vacuum fields, Angew. Chem., Int. Ed. Engl. **51**, 1592 (2012).

Supporting Information: Manipulating Core-Excitations in Molecules by X-ray Cavities

Bing Gu, ^{1,*} Artur Nenov, ^{2,*} Francesco Segatta, ² Marco Garavelli, ^{2,†} and Shaul Mukamel ^{1,‡}

¹Department of Chemistry and Department of Physics and Astronomy,

University of California, Irvine, 92697, USA

²Dipartimento di Chimica Industriale "Toso Montanari",

Università degli studi di Bologna, Viale del Risorgimento 4, 40136 Bologna, Italy.

^{*} These authors contributed equally to this work.

 $^{^{\}dagger}$ marco.garavelli@unibo.it

 $^{^{\}ddagger}$ smukamel@uci.edu

CONTENTS

S1. DERIVATION OF EQ. (2)

Under the rotating-wave and long-wavelength approximations,

$$H_{\rm CM} = \mathbf{V}^{\dagger} \cdot \hat{\mathbf{E}}^{(+)}(\mathbf{r} = 0) + \text{H.c.}$$
 (S1)

where \mathbf{V} and \mathbf{V}^{\dagger} are, respectively, the lowering and raising dipole operator $\mathbf{V} + \mathbf{V}^{\dagger} = -\sum_{n} \boldsymbol{\mu}^{(n)}$ and $\hat{\mathbf{E}}^{(+)}(\mathbf{r})$ ($\hat{\mathbf{E}}^{(-)}(\mathbf{r})$) is the positive (negative)-frequency component of the electric field operator.

With the collective states

$$|C_{\alpha k}\rangle = \frac{1}{\sqrt{N}} \sum_{k} e^{ikn} |c_{\alpha}^{(n)}\rangle,$$
 (S2)

for c=e,f and $k=2\pi j/N, j=0,\cdots,N-1$, the local core-excitation states (in the many-body space) can be rewritten as

$$|c_{\alpha}^{(n)}\rangle = \frac{1}{\sqrt{N}} \sum_{k} e^{-ikn} |C_{\alpha k}\rangle$$
 (S3)

Up to double excitations, the relevant molecular states contain $|G\rangle$, $|E_{\alpha k}\rangle$, $|F_{\beta k}\rangle$, $|e_{\alpha}^{(n)}e_{\beta}^{(m)}\rangle$, $n \neq m$. Within this subspace, inserting Eq. (S3) into the cavity-molecule coupling yields Eq. (2)

$$H_{\text{CM}} = \sum_{k} \sum_{n} \kappa_{e_{\alpha}g} \frac{1}{\sqrt{N}} e^{-ikn} |E_{\alpha k}\rangle \langle G| a + \sum_{\alpha,\beta} \sum_{k,k'} \sum_{n} \frac{1}{N} e^{-i(k-k')n} \kappa_{f_{\beta}e_{\alpha}} |F_{\beta k}\rangle \langle E_{\alpha k'}| a$$

$$+ \sum_{n \neq m} \sum_{\alpha,\gamma} \kappa_{e_{\alpha}g} |e_{\alpha}^{(n)} e_{\gamma}^{(m)}\rangle \langle e_{\gamma}^{(m)}| a + \text{H.c.}$$

$$= \sum_{\alpha} \kappa_{e_{\alpha}g} \sqrt{N} |E_{\alpha 0}\rangle \langle G| a + \sum_{\alpha,\beta} \sum_{k} \kappa_{f_{\beta}e_{\alpha}} |F_{\beta k}\rangle \langle E_{\alpha k}| a + \sum_{n \neq m} \sum_{\alpha,\gamma} \kappa_{e_{\alpha}g} |e_{\alpha}^{(n)} e_{\gamma}^{(m)}\rangle \langle e_{\gamma}^{(m)}| + \text{H.c.}$$
(S4)

where $\kappa_{ji} = \sqrt{\hbar \omega_{\rm c}/2\varepsilon_0 V_{\rm c}} \langle j | \boldsymbol{\mu} \cdot \mathbf{e}_{\rm c} | i \rangle$.

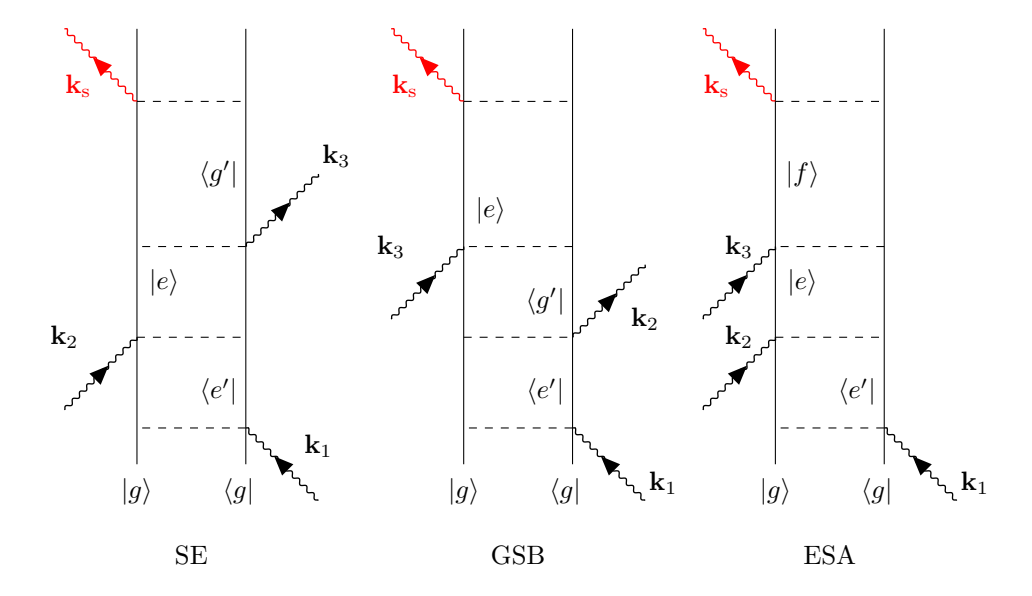


FIG. S1. Three double-sided Feynman diagrams for the 2D photon echo signal. GSB: ground state bleaching; SE: stimulated emission; ESA: excited state absorption.

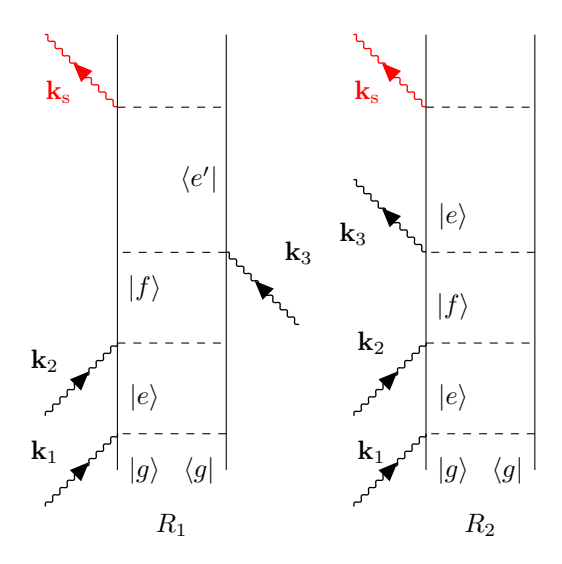


FIG. S2. Two double-sided Feynman diagrams contributing to the 2D double quantum coherence signal. The pump pulses \mathbf{k}_1 and \mathbf{k}_2 brings the system to a double-quantum coherence $|f\rangle\langle g|$.

S2. ELECTRONIC STRUCTURE SIMULATIONS

The ground state (g) and the manifolds of singly (e) and doubly (f) core-excited states of 1,1-diffuoroethylene cannot be computed in one shot as they are energetically separated by several hundreds of eV (carbon K-edge is around 290 eV above the ground state (GS), whereas the f manifold contains states absorbing around 580 eV. This implies that a number of electronic states, irrelevant to the issue under scrutiny, are situated in between the manifolds.

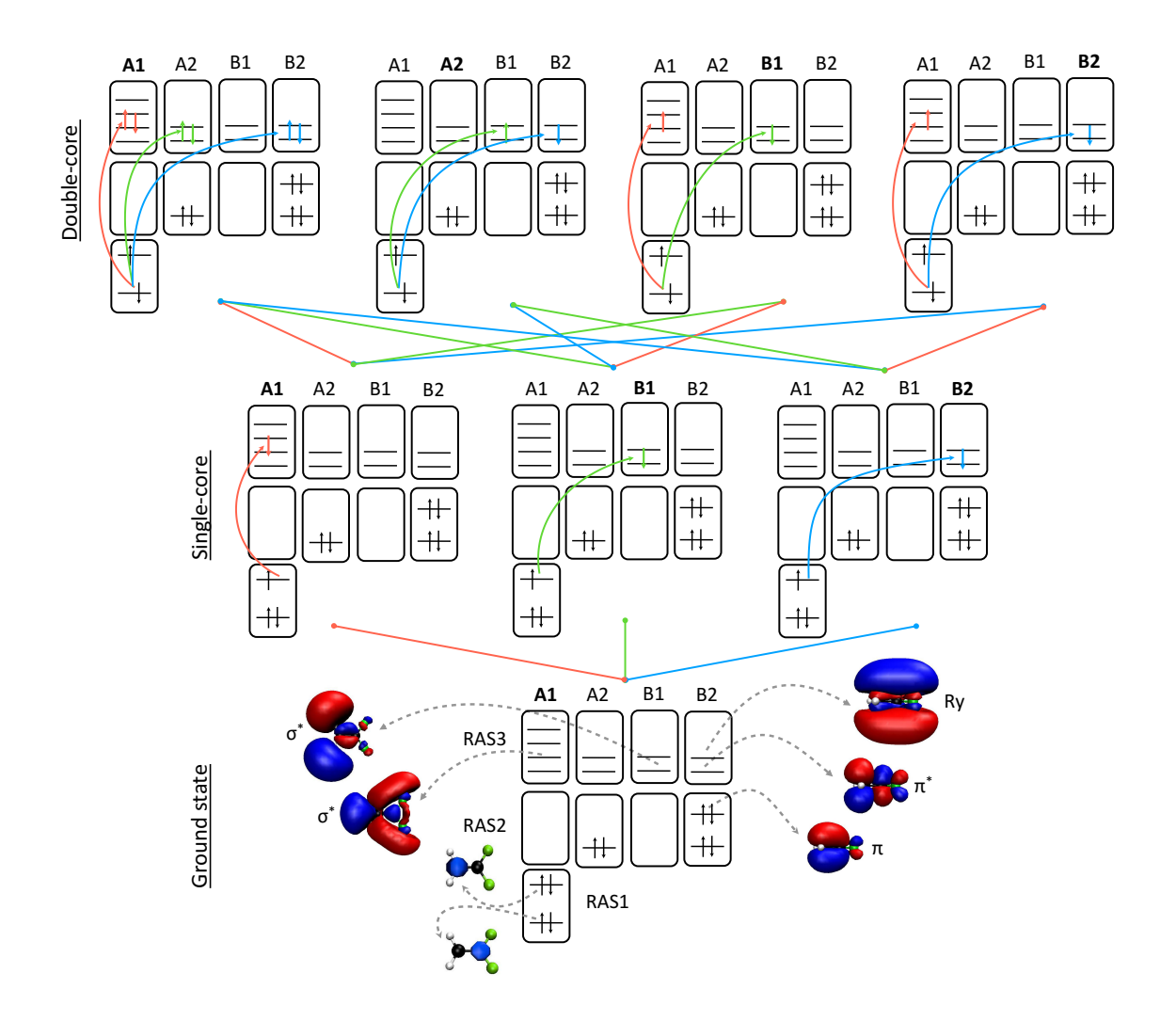


FIG. S3. Scheme showing the ground state, single- and double-core excited manifolds (grouped by symmetry) of 1,1-diffuoroethylene with the restricted active space RAS(10, 2, 4; 2, 3, 10) defined in the text. The various transitions connecting the manifolds are depicted and highlighted in color according to the irreducible representation to which the orbitals involved in the corresponding $g \to e$ or $e \to f$ transition belong, namely A1 (red) B1 (green) and B2 (blue). Each of the eight electronic configurations shown requires a separate calculation, each arrow denotes a non-zero transition dipole vector between manifolds. Representative orbitals of the active space are also shown.

The strategy to target single- and double-core excitations used here is based on the restricted active space self consistent field (RASSCF) approach [1] from the family of multi-configuration wavefunction based methods. In a nutshell, RASSCF subdivides the full active space (AS) into three subspaces: RAS1, with a fixed upper limit of holes; RAS2, where all possible permutations of electrons within the orbitals are considered; RAS3, with a maximal number of electrons. The possible configuration state functions (CSF's) over which the wavefunction is expanded, are built

according to these rules. A projection technique denoted *highly excited states* (HEXS) which selectively removes CSF's with a certain occupation from a given subspace is used to effectively project out undesired valence transitions preceding energetically the core transitions.[2]. The dynamical correlation missing at the RASSCF level is recovered through multireference second-order perturbation corrections (RASPT2).[3–5]

Below we outline the protocol for computing both linear and non-linear spectra. To speed up the calculations, we have taken advantage of the C_{2h} symmetry of the molecule.

The AS is constructed as follows (Fig. S5).

- RAS1: contains both core-orbitals which are kept frozen to avoid orbital rotation during the variational optimization of the MO coefficients; the upper limit of holes is set to 2;
- RAS2: three π -type occupied orbitals are placed herein (one in irreducible representations A1 and two in B2)
- RAS3: 10 virtual orbitals are included (four, two, two and two in irreducible representations A1, A2, B1 and B2, respectively). The maximum of excitations in this sub-space was set to four.

In the following we designate the active space as RAS(10, 2, 4; 2, 3, 10), where the first three indices denote the number of electrons, the upper limit of holes (in RAS1) and the upper limit of excitations (in RAS3), respectively; while the last three indies denotes the number of orbitals included in the three subspaces: in order, RAS1, RAS2 and RAS3.

The construction of the RAS3 space is vital for the completeness of the spectrum as every virtual orbital is potentially the source of a core-excited state and, consecutively, of a signal. Its composition was determined in the following way. First, preliminary calculations were run for each of the three symmetries A1, B1 and B2 (states of the A2 symmetry are not coupled to the GS) where up to ten virtual orbitals were included in the corresponding irreducible representation and up to 15 states were computed at the RASSCF/RASPT2 level[6]. Subsequently, the nature of the transitions comprising the carbon K-edge of the XANES spectrum up to 296 eV was analyzed in order to identify the virtual orbitals giving rise to the leading CSF's in the multiconfigurational wavefunctions involved in the identified transitions. The RAS(10, 2, 4; 2, 3, 10) was constructed by limiting RAS3 to the virtual orbitals identified through the aforementioned analysis. Finally, it was verified that the results obtained with the RAS(10, 2, 4; 2, 3, 10) reproduce the transitions identified previously.

The same RAS(10, 2, 4; 2, 3, 10) was utilized to obtain the g, e and f manifolds[7]. The GS was computed in a state-specific calculation. The e manifold consisting of six states of A1, four states of B1 and three states of B2 symmetry was obtained by selectively removing all CSF's with a full (i.e. four electrons) occupation in the RAS1 subspace[8]. Finally, the f manifold consisting of twelve states in each of the four symmetries of the D_{2h} point group was obtained by removing all CSF's with four and three electrons in the RAS1 subspace. Thus, the total Hamiltonian is constructed of 62 electronic states: one GS, 13 single core-excitations and 48 double-core excitations. We note, that in the calculation of the GS and f manifold orbital relaxation was restricted only within the active space when (thus effectively prohibiting rotations out of the AS) in order to preserve the composition of the AS. Benchmarking against calculation where the orbitals were allowed to relax freely. Figure S4 shows that this restriction does not affect the final spectra.

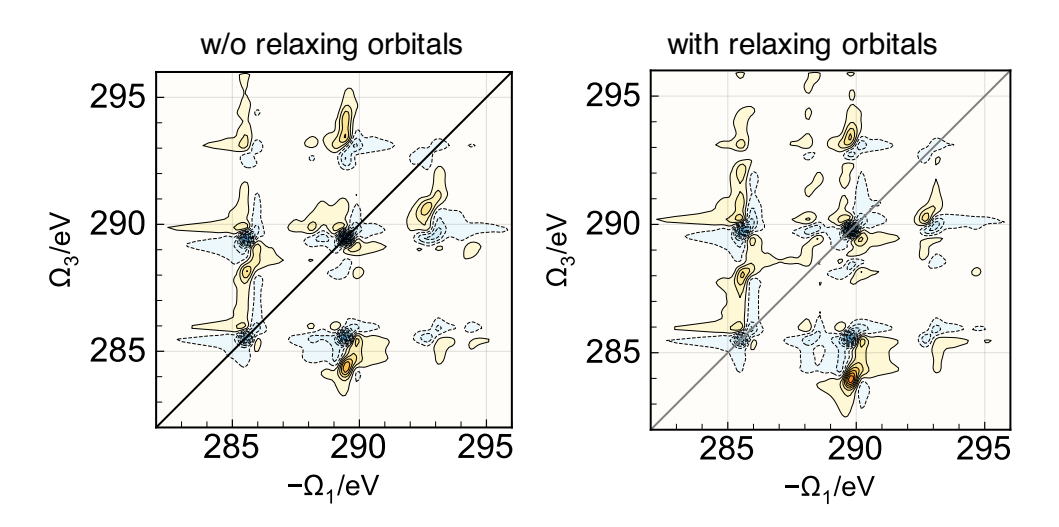


FIG. S4. Photon echo signal for 1,1-difluoroethylene when the orbitals in the active space are frozen (left) and when they are allowed to relax (right).

Multi state (MS)-RASPT2 was performed on top of each RASSCF calculation to account for the dynamical correlation, setting the ionization-potential electron-affinity shift [9, 10] of $0.0 E_h$. Core orbitals were explicitly correlated. To reduce problems with intruder states an imaginary shift [11] of $0.3 E_h$ has been applied.

Transition dipole moments between the g, e and f manifolds were computed by means of biorthogonalization through the RAS state interaction (SI) routine. The protocol is summarized in Fig. S3

Scalar relativistic effects have been included by using a second-order Douglas-Kroll-Hess Hamiltonian in combination with a relativistic atomic natural orbital basis set, ANO-RCC.[12] A triple- ζ

basis function set augmented with two sets of d-functions for carbon and fluorine atoms and a set of f-functions for fluorine, thus giving rise to ANO-RCC: C[4s3p2d], F[4s3p2d1f], H[2s1p]. A density-fitting approximation of the electron repulsion integrals has been used, knows as Cholesky decomposition.[13]

All calculations were performed in the gas-phase with the OpenMolcas suite. [14, 15]

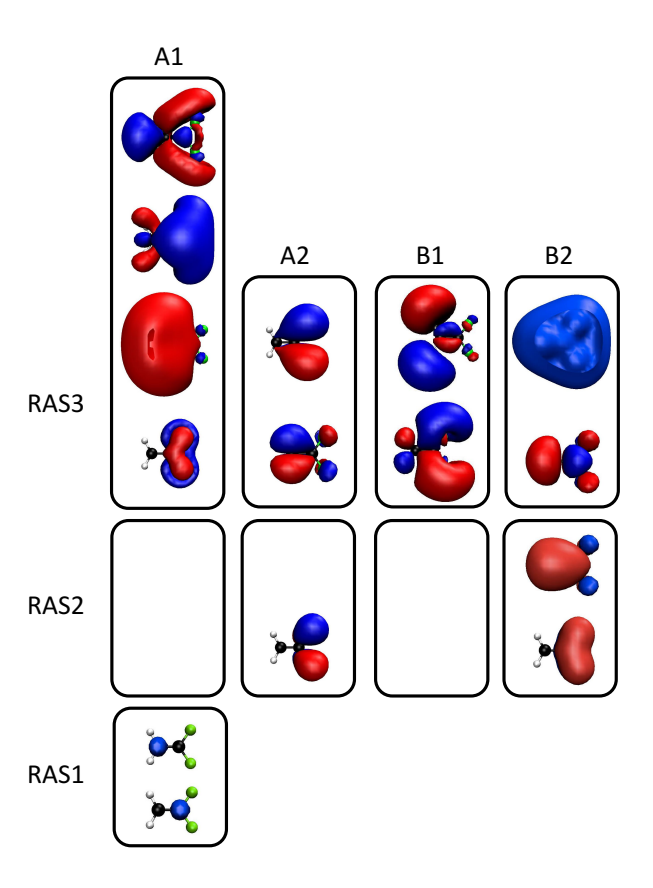


FIG. S5. Orbitals from the active space RAS(10; 2; 4; 2; 3; 10).

S3. SIMULATIONS OF SPECTRA

The XAS, PE and DQC signals are calculated using the sum-over-states (SOS) protocol. The SOS formula for XAS is given below in Eq. (S9). Expressions for the 2D-PE and 2D-DQC can be derived similarly, details can be found in Ref. [16]. The lifetime broadening of the core-polariton is accounted for by a decay constant $\gamma_{ji} = 0.3 \,\text{eV}$. We use attosecond pulses with central frequency around $\omega_j^0 = 288 \,\text{eV}$ for all j and bandwidth 15 eV such that $E_j(\omega_j) \approx E_j(\omega_j^0)$ for $\omega \in (285, 296)$ eV. Such pulses can be generated by free-electron lasers [17]. All the interactions between external laser pulses and molecules are assumed in the perturbative regime.

The single-polariton and two-polariton states are computed by diagonalizing the polariton Hamiltonian represented in the direct-product electronic-photonic basis $|\alpha n\rangle \equiv |\alpha\rangle \otimes |n\rangle$ up to double excitations, where α denotes electronic state and n is the photon number state. For XANES, we consider N molecules and include the collective core-excited state $\{ |E_{\alpha 0}0\rangle, |G1\rangle \}$. For 2D-PE and 2D-DQC spectra, we consider a single molecule and include $\{|f0\rangle, |e1\rangle, |g2\rangle\}$.

In the DQC simulations for $S(\Omega_2, \Omega_1; T_3)$, we focus on $T_3 \approx 0$. In practice, a very small number $\sim 1 \times 10^{-5}$ as is used to avoid cancellation of the two diagrams at $T_3 = 0$. And similarly for $S(\Omega_3, \Omega_2; T_1)$.

S3.A. Sum-over-states expression for XANES

We adopt a superoperator notation where the density matrix is written as a vector $\rho = \sum_{ij} \rho_{ij} |i\rangle \langle j| \rightarrow \sum_{ij} \rho_{ij} |ij\rangle \rangle$, and $\mathcal{V}_{L}\rho \equiv V\rho$, $\mathcal{V}_{R}\rho \equiv \rho V$ are, respectively, the left and right superoperators, $\mathcal{V}_{\pm}\rho \equiv [V,\rho]_{\pm}$ the commutator and anticommutator [18]. We assume a fixed polarization and suppress the vector notation of the dipole and electric fields.

X-ray absorption near edge structure (XANES) uses a single x-ray pulse

$$E(t) = \int_0^\infty d\omega E(\omega) e^{-i\omega t} + \text{c.c.}.$$
 (S5)

The Feynman diagram for XANES is shown in Fig. 1 and the corresponding expression reads

$$\langle V(t) \rangle = \int_0^\infty d\tau \langle \langle V^{\dagger} | \mathcal{G}(\tau) \mathcal{V}_{L}^{\dagger} | gg \rangle \rangle E(t - \tau)$$
 (S6)

where $\mathcal{G}(t-t') = -i\theta(t-t')e^{-i\mathcal{L}(t-t')}$ with the Liouvillian $\mathcal{L}\rho = [H,\rho]$ is the Green's function for the Liouville-von Neumann equation. Inserting Eq. (S5) into Eq. (S6) leads to

$$\langle V(t)\rangle = \int_0^\infty \frac{\mathrm{d}\omega}{2\pi} \frac{\mu_{ge}\mu_{eg}}{\omega - \omega_{eg} + i\gamma_{eg}} E(\omega) e^{-i\omega t} = -i\theta(t)\mu_{eg}\mu_{ge} E(\omega_{eg} - i\gamma_{eg}) e^{-i\omega_{eg}t - \gamma_{eg}t}$$
(S7)

where $\omega_{ij} \equiv \omega_i - \omega_j$, μ_{ij} are respectively the transition energies, transition dipole moments for coreexcitations without the cavity, and for core-polaritons inside the cavity. In the second equality in Eq. (S7), we have extended the lower integration limit to $-\infty$ since $E(\omega)$ is localized around a central frequency in the X-ray regime, and then used Cauchy's integral formula in the lower half circle. Inserting Eq. (S7) into the frequency-dispersed signal (photon flux into each frequency photon mode)

$$S_{\rm XAS}(\omega) = -2 \operatorname{Im} \langle V(\omega) \rangle E^*(\omega),$$
 (S8)

where $\mathbf{V}(\omega) = \int_{-\infty}^{+\infty} \mathrm{d}t \mathbf{V}(t) e^{i\omega t} (\mathbf{E}^*(\omega))$ is the Fourier transform of $\mathbf{V}(t)$ ($\mathbf{E}^*(t)$), the negative-frequency component of the electric field), leads to the sum-over-states expression

$$S_{\rm XAS}(\omega) = -2 \operatorname{Im} \sum_{e} \frac{\mu_{eg} \mu_{ge} E(\omega_{eg} - i\gamma_{eg}) E^*(\omega)}{\omega - \omega_{eg} + i\gamma_{eg}}$$
 (S9)

S4. TWO-PHOTON ABSORPTION

In two-photon absorption (TPA), the system is excited from the ground state to two-polariton states by simultaneously absorbing two photons. The TPA employs two laser pulses with electric field

$$E(t) = E_1 e^{-i\omega_1 t} + E_2 e^{-i\omega_2 t} + \text{c.c.},$$
 (S10)

and the signal can be defined as the transition rate to the final states $|f\rangle$, $S_{\text{TPA}} = \lim_{t\to\infty} \sum_f \frac{\mathrm{d}P_f(t)}{\mathrm{d}t}$ where $P_f(t) = \text{Tr}\left\{\rho(t)|f\rangle\langle f|\right\}$. The time-loop diagrams for TPA are shown in Fig. S6, and the expression is given by [19]

$$S_{\text{TPA}} = \delta(\omega_f - \omega_1 - \omega_2)|E_1 E_2|^2 \left| \sum_e \frac{\mu_{fe} \mu_{eg}}{\omega_1 - \omega_e + i\gamma_e} + \frac{\mu_{fe} \mu_{eg}}{\omega_2 - \omega_e + i\gamma_e} \right|^2$$
 (S11)

where e runs over the intermediate single-polariton states.

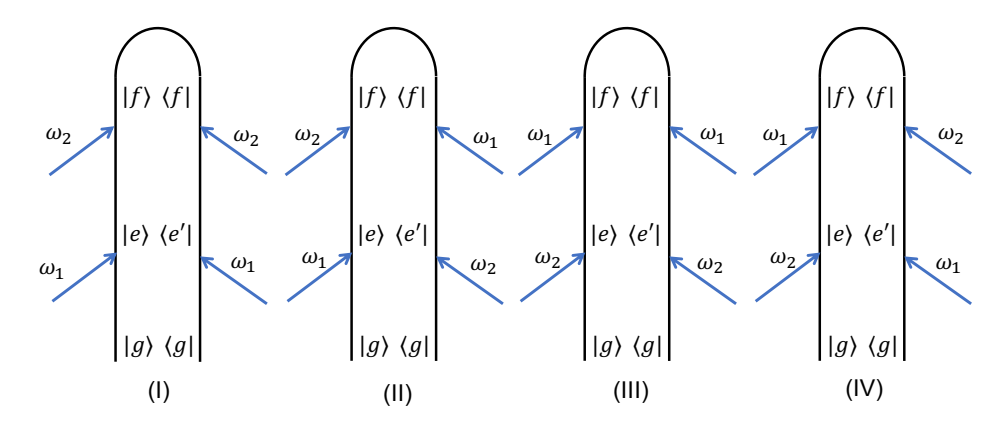


FIG. S6. Time-loop diagrams for the two-photon absorption signal. The four diagrams arise from the time-ordering of the four interactions along time-loop counterclockwise.

Figure S7 shows the TPA spectra $S_{\text{TPA}}(\omega_1 + \omega_2, \omega_1)$ for bare molecules and for the corepolaritons. The peaks show the correlation between the bipolariton states $|f\rangle$ and the singlepolariton states $|e\rangle$. The y-axis shows the bipolariton resonances ω_{fg} and the x-axis shows the transition energy either between the single-polariton and the ground state ω_{eg} or between the

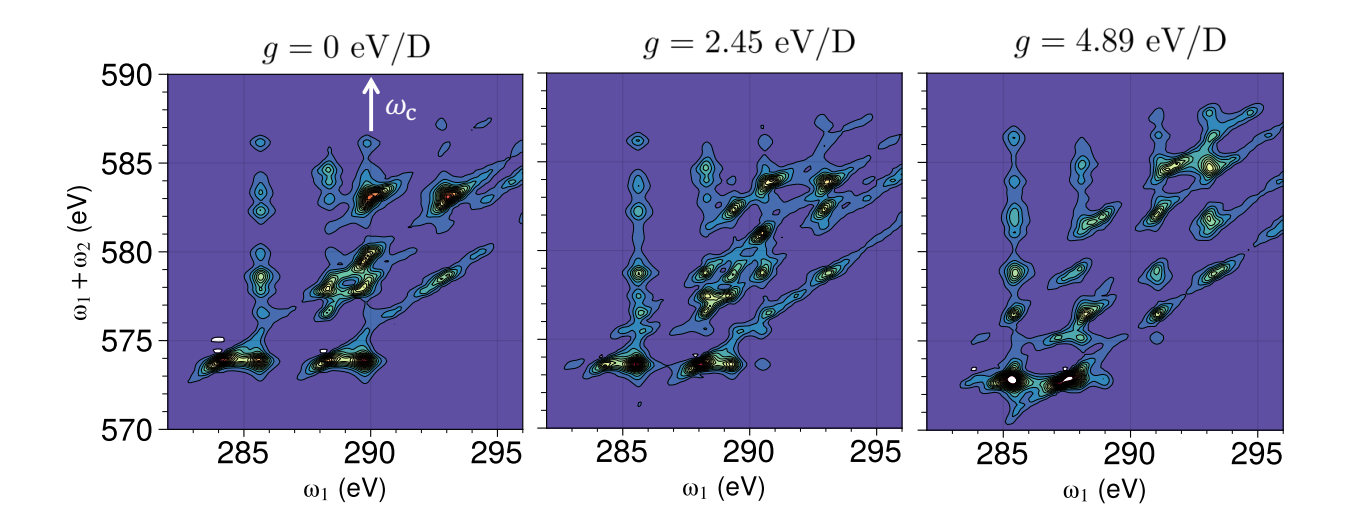


FIG. S7. Two-photon absorption spectra $S_{\text{TPA}}(\Omega_1 + \omega_2, \Omega_1)$ for (a) bare molecule and for (b,c) corepolaritons of 1,1-difluoroethylene in an X-ray cavity. Here $\omega_c = 290\,\text{eV}$, and the coupling strength g is indicated.

bipolariton state and the single-polariton state ω_{fe} . The latter corresponds to the system absorbing ω_2 first and then absorbing ω_1 to the final state. The TPA spectra provide similar information as the double quantum coherence signal.

[1] Per-Ake Malmqvist, Alistair Rendell, and Björn O. Roos, "The restricted active space self-consistent-field method, implemented with a split graph unitary group approach," J. Phys. Chem. **94**, 5477–5482 (1990).

[2] Marcus Lundberg and Mickaël G. Delcey, *Transition Metals in Coordination Environments*, edited by Ewa Broclawik, Tomasz Borowski, and Mariusz Radoń (Springer International Publishing, 2019) Chap. Multiconfigurational Approach to X-ray Spectroscopy of Transition Metal Complexes.

[3] Kerstin Andersson, Per-Ake Malmqvist, Bjoern O. Roos, Andrzej J. Sadlej, and Krzysztof Wolinski, "Second-order perturbation theory with a CASSCF reference function," J. Phys. Chem. **94**, 5483–5488 (1990).

[4] Vicenta Sauri, Luis Serrano-Andrés, Abdul R. M. Shahi, Laura Gagliardi, Steven Vancoillie, and Kristine Pierloot, "Multiconfigurational second-order perturbation theory restricted active space (RASPT2) method for electronic excited states: A benchmark study." J. Chem. Theory Comput. 7, 153 (2011).

[5] Daniel Roca-Sanjuán, Francesco Aquilante, and Roland Lindh, "Multiconfiguration second-order perturbation theory approach to strong electron correlation in chemistry and photochemistry," Wiley Interdiscip. Rev. Comput. Mol. Sci. 2, 585–603 (2011).

[6] Details on the RASPT2 parameters are given below.

- [7] The use of a uniform AS for all manifolds is a requirement for computing the transition dipole moments μ_{eg} and μ_{fe} .
- [8] Note that the states belonging to each irreducible representation have to be computed in a separate state-average calculation.
- [9] Giovanni Ghigo, Björn O. Roos, and Per-Ake Malmqvist, "A modified definition of the zeroth-order Hamiltonian in multiconfigurational perturbation theory (CASPT2)," Chem. Phys. Lett. 396, 142–149 (2004).
- [10] J. Patrick Zobel, Juan J. Nogueira, and Leticia González, "The IPEA dilemma in CASPT2," Chem. Sci. 8, 1482–1499 (2017).
- [11] Niclas Forsberg and Per-Ake Malmqvist, "Multiconfiguration perturbation theory with imaginary level shift," Chem. Phys. Lett. **274**, 196–204 (1997).
- [12] Björn O. Roos, Valera Veryazov, and Per-Olof Widmark, "Relativistic atomic natural orbital type basis sets for the alkaline and alkaline-earth atoms applied to the ground-state potentials for the corresponding dimers," Theor. Chem. Acc. 111, 345–351 (2004).
- [13] Thomas Bondo Pedersen, Francesco Aquilante, and Roland Lindh, "Density fitting with auxiliary basis sets from Cholesky decompositions," Theor. Chem. Acc. **124**, 1–10 (2009).
- [14] Ignacio Fdez. Galván, Morgane Vacher, Ali Alavi, Celestino Angeli, Francesco Aquilante, Jochen Autschbach, Jie J. Bao, Sergey I. Bokarev, Nikolay A. Bogdanov, Rebecca K. Carlson, Liviu F. Chibotaru, Joel Creutzberg, Nike Dattani, Mickaël G. Delcey, Sijia S. Dong, Andreas Dreuw, Leon Freitag, Luis Manuel Frutos, Laura Gagliardi, Frédéric Gendron, Angelo Giussani, Leticia González, Gilbert Grell, Meiyuan Guo, Chad E. Hoyer, Marcus Johansson, Sebastian Keller, Stefan Knecht, Goran Kovačević, Erik Källman, Giovanni Li Manni, Marcus Lundberg, Yingjin Ma, Sebastian Mai, João Pedro Malhado, Per Åke Malmqvist, Philipp Marquetand, Stefanie A. Mewes, Jesper Norell, Massimo Olivucci, Markus Oppel, Quan Manh Phung, Kristine Pierloot, Felix Plasser, Markus Reiher, Andrew M. Sand, Igor Schapiro, Prachi Sharma, Christopher J. Stein, Lasse Kragh Sørensen, Donald G. Truhlar, Mihkel Ugandi, Liviu Ungur, Alessio Valentini, Steven Vancoillie, Valera Veryazov, Oskar Weser, Tomasz A. Wesołowski, Per-Olof Widmark, Sebastian Wouters, Alexander Zech, J. Patrick Zobel, and Roland Lindh, "OpenMolcas: From Source Code to Insight," J. Chem. Theory Comput. 15, 5925–5964 (2019).
- [15] Francesco Aquilante, Jochen Autschbach, Alberto Baiardi, Stefano Battaglia, Veniamin A. Borin, Liviu F. Chibotaru, Irene Conti, Luca De Vico, Mickaël Delcey, Ignacio Fdez. Galván, Nicolas Ferré, Leon Freitag, Marco Garavelli, Xuejun Gong, Stefan Knecht, Ernst D. Larsson, Roland Lindh, Marcus Lundberg, Per Åke Malmqvist, Artur Nenov, Jesper Norell, Michael Odelius, Massimo Olivucci, Thomas B. Pedersen, Laura Pedraza-González, Quan M. Phung, Kristine Pierloot, Markus Reiher, Igor Schapiro, Javier Segarra-Martí, Francesco Segatta, Luis Seijo, Saumik Sen, Dumitru-Claudiu Sergentu, Christopher J. Stein, Liviu Ungur, Morgane Vacher, Alessio Valentini, and Valera Veryazov, "Modern quantum chemistry with [Open]Molcas," J. Chem. Phys. 152, 214117 (2020).

- [16] Markus Kowalewski, Benjamin P. Fingerhut, Konstantin E. Dorfman, Kochise Bennett, and Shaul Mukamel, "Simulating Coherent Multidimensional Spectroscopy of Nonadiabatic Molecular Processes: From the Infrared to the X-ray Regime," Chem. Rev. 117, 12165–12226 (2017).
- [17] C. Pellegrini, A. Marinelli, and S. Reiche, "The physics of x-ray free-electron lasers," Rev. Mod. Phys. 88, 015006 (2016).
- [18] Konstantin E. Dorfman and Shaul Mukamel, "Nonlinear spectroscopy with time- and frequency-gated photon counting: A superoperator diagrammatic approach," Phys. Rev. A 86, 013810 (2012).
- [19] Bing Gu and Shaul Mukamel, "Manipulating Two-Photon-Absorption of Cavity Polaritons by Entangled Light," J. Phys. Chem. Lett. 11, 8177–8182 (2020).